Strain Engineering of Graphene's Electronic Structure

Vitor M. Pereira and A. H. Castro Neto

Department of Physics, Boston University, 590 Commonwealth Avenue, Boston, Massachusetts 02215, USA
(Received 13 February 2009; published 20 July 2009)

We explore the influence of local strain on the electronic structure of graphene. We show that strain can be easily tailored to generate electron beam collimation, 1D channels, surface states, and confinement. These can be seen as basic elements for all-graphene electronics which, by suitable engineering of local strain profiles, could be integrated on a single graphene sheet. In addition this proposal has the advantage that patterning can be made on substrates rather than on graphene, thereby protecting the integrity of the latter.

Notwithstanding its atomic thickness, graphene sheets have been shown to accommodate a wealth of remarkable fundamental properties, and to hold sound prospects in the context of a new generation of electronic devices and circuitry [1]. One exciting prospect about graphene is that, not only can we have extremely good conductors, but also most active devices made out of graphene. Current difficulties with respect to this goal lie in that conventional electronic operations require the ability to completely pinch off the charge transport on demand. Although the electric field effect is impressive in graphene [2], the existence of a minimum of conductivity poses a serious obstacle towards desirable on/off ratios. A gapped spectrum would certainly be instrumental. The presence of a gap is implicitly related to the problem of electron confinement, which for Dirac fermions is not easily achievable by conventional means (like electrostatic potential wells) [3]. Geometrical confinement has been achieved in graphene ribbons and dots [4,5], but the sensitivity of transport to the edge profile [6], and the inherent difficulty in the fabrication of such microstructures with sharply defined edges remains a problem.

The ultimate goal would be an all-graphene circuit. This could be achieved by taking a graphene sheet and patterning the different devices and leads by means of appropriate cuts that would generate leads, ribbons, dots, etc. This *paper cutting* electronics can have serious limitations with respect to reliability, scalability, and is prone to damaging and inducing disorder in the graphene sheet [7]. Therefore, in keeping with the paper art analogy, we propose an alternative *origami* electronics [8].

We show here that all of the characteristics of graphene ribbons and dots (viz. geometrical quantization, 1D channels, surface modes) might be locally obtained by patterning, *not graphene*, but the substrate on which it rests. The essential aspect of our approach is the generation of strain in the graphene lattice capable of changing the in-plane hopping amplitude in an anisotropic way. This can be achieved by means of appropriate geometrical patterns in a homogeneous substrate (grooves, creases, steps, or wells), by means of a heterogeneous substrate in which

different regions interact differently with the graphene sheet, generating different strain profiles [Fig. 1(b)]. Another design alternative consists in depositing graphene onto substrates with regions that can be controllably strained on demand [9], or by exploring substrates with thermal expansion heterogeneity. Through a combination of folding and/or clamping a graphene sheet onto such substrates, one might generate local strain profiles suitable for the applications discussed in detail below, while preserving a whole graphene sheet.

The remainder of the Letter is dedicated to showing how strain only can be used as a means of achieving (i) direction dependent tunneling, (ii) beam collimation, (iii) confinement, (iv) the spectrum of an effective ribbon, (v) 1D channels, and (vi) surface modes.

Model.—Within a tight-binding formulation of the electronic motion [10], effects of in-plane strain can be captured, to leading order, by considering the changes in nearest-neighbor hopping amplitude, t. We write $t(\boldsymbol{R}_i, \boldsymbol{n}) = t + \delta t(\boldsymbol{R}_i, \boldsymbol{n})$, and treat the space dependent strain-induced modulation, δt, as a perturbation ($t \approx 3$ eV). It is straightforward to show [10] that, for smooth perturbations, the low energy Hamiltonian is

$$H = v_F \int d\boldsymbol{r} \Psi^\dagger \begin{bmatrix} \boldsymbol{\sigma} \cdot \left(\boldsymbol{p} - \frac{1}{v_F}\mathcal{A}\right) & 0 \\ 0 & -\boldsymbol{\sigma} \cdot \left(\boldsymbol{p} + \frac{1}{v_F}\mathcal{A}\right) \end{bmatrix} \Psi,$$

(1)

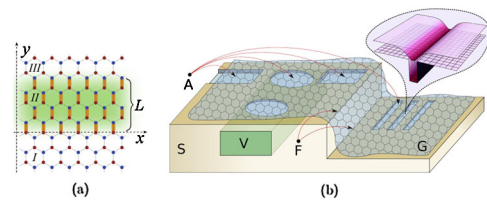valid near the valleys K and K' in the Brillouin zone, with

FIG. 1 (color online).   (a) Lattice orientation considered in the text. Thicker bonds have perturbed hopping. (b) Artistic depiction of a substrate (S) patterned with folds (F), trenches, dots and wells (A), upon which rests a graphene sheet (G).

$\boldsymbol{\sigma} = (\sigma_x, \sigma_y, \sigma_z)$, $v_F = 3ta/2\hbar$ and $\Psi = (\psi_K^A(\boldsymbol{r}), \psi_K^B(\boldsymbol{r}), \psi_{K'}^B(\boldsymbol{r}), \psi_{K'}^A(\boldsymbol{r}))^\dagger$ is a spinor containing the electron fields in each sublattice and valley. Within each valley it has the form $H = v_F \boldsymbol{\sigma} \cdot (\boldsymbol{p} - \frac{1}{v_F}\mathcal{A})$, so that electron dynamics is determined by a Dirac equation in the presence of a gauge field $\mathcal{A}$. This field stems from the perturbation to the homogeneous hopping amplitudes and is related to $\delta t(\boldsymbol{R}, \boldsymbol{n})$ via the complex vector potential (VP):

$$\mathcal{A}_x(\boldsymbol{r}) - i\mathcal{A}_y(\boldsymbol{r}) = \sum_{\boldsymbol{n}} \delta t(\boldsymbol{r}, \boldsymbol{n})e^{i\boldsymbol{K}\cdot\boldsymbol{n}}. \qquad (2)$$

The fact that $\mathcal{A}$ appears in (1) with its sign reversed for the K' valley guarantees overall time reversal symmetry. For definiteness, with the lattice orientation shown in Fig. 1(a) we perturb the vertical hopping by a constant amount δt, over a finite region of width L. The perturbation and the associated $\mathcal{A}(\boldsymbol{r})$ are

$$\delta t(\boldsymbol{R}_i, \boldsymbol{n}) = \delta t \delta_{\boldsymbol{n},0} \theta(Y_i)\theta(L - Y_i), \qquad (3a)$$
$$\mathcal{A}(\boldsymbol{r}) = \delta t \theta(y)\theta(L - y)\boldsymbol{u}_x. \qquad (3b)$$

The gauge field $\mathcal{A}$ is oriented along $\boldsymbol{u}_x$, which coincides with the direction of translational invariance. Using units where $v_F = \hbar = 1$, and allowing for the presence of an electrostatic potential $V(\boldsymbol{r})$ in the barrier region, the wave equations for the K valley can then be cast as

$$[-i\partial_x - \partial_y - \mathcal{A}_x(y)]\psi^B(\boldsymbol{r}) = [E - V(\boldsymbol{r})]\psi^A(\boldsymbol{r}), \qquad (4a)$$
$$[-i\partial_x + \partial_y - \mathcal{A}_x(y)]\psi^A(\boldsymbol{r}) = [E - V(\boldsymbol{r})]\psi^B(\boldsymbol{r}). \qquad (4b)$$

In this formulation, the problem reduces to the study of Dirac electrons in the presence of VP and electrostatic barriers, and is related to corresponding studies of Dirac electrons in the presence of magnetic barriers [11–14]. The profile (3b) has also been considered in Ref. [15] in modeling a suspended graphene sheet.

Tunneling.—We begin by analyzing the tunneling characteristics across the barrierlike perturbation of Eq. (3). Without compromising generality [16], in the remainder of the Letter we shall be concerned with the situation $\delta t > 0$ and $E > 0$. We parametrize the wave function in the three regions of Fig. 1(a) as

$$\Psi^{\mathrm{I}} = e^{ik_x x + ik_y y}\begin{pmatrix} 1 \\ e^{i\phi} \end{pmatrix} + Re^{ik_x x - ik_y y}\begin{pmatrix} 1 \\ e^{-i\phi} \end{pmatrix},$$

$$\Psi^{\mathrm{II}} = C_1\begin{pmatrix} 1 \\ e^{i\varphi} \end{pmatrix}e^{ik_x x + iq_y y} + C_2\begin{pmatrix} 1 \\ e^{-i\varphi} \end{pmatrix}e^{ik_x x - iq_y y},$$

$$\Psi^{\mathrm{III}} = Te^{ik_x x + ik_y y}\begin{pmatrix} 1 \\ e^{i\phi} \end{pmatrix},$$

where we have the kinetic momenta $k_x = E\cos\phi$, $k_x - \delta t = E\cos\varphi$, $q_y = E\sin\varphi$, and the energy $E^2 = k_x^2 + k_y^2 = (k_x - \delta t)^2 + q_y^2$. Substitution in the wave equation (4) leads to the following transmission amplitude [13,15]:

$$T = \frac{e^{-ik_y L}\sin\phi \sin\varphi}{\cos(q_y L)\sin\phi \sin\varphi + i\sin(q_y L)(\cos\phi \cos\varphi - 1)}. \qquad (5)$$

This result is valid also for $V \neq 0$ with the appropriate substitution $E \to E - V$ inside the barrier. As pointed out in the case of a real magnetic field [17], conservation of k_x requires $E\cos\phi = \delta t + E\cos\varphi$, leading to strong suppression of tunneling for $\phi > \arccos(-1 + \delta t/E)$. When such a condition is in effect, the internal angle has to be analytically continued to the imaginary axis $\varphi \to i\varphi$, $q_y \to iq_y$ causing an exponential suppression of $|T|^2$. Moreover, if $\delta t/E > 2$ tunneling is completely suppressed. These effects are illustrated in Fig. 2(a) where we plot $|T|^2$ for different values of L and V.

Beam collimation.—Several aspects can be immediately identified from Fig. 2. Klein tunneling [3] is absent for a pure VP barrier, and if $V \neq 0$ Klein tunneling might persist albeit at $\phi \neq \pi/2$. As hinted above, for wide barriers tunneling is highly suppressed for certain ranges of ϕ that depend on δt, E, and V. This filtering effect for certain incidence angles is best appreciated by inspecting the phase-space pictures shown in Fig. 2(b): the effect of $\mathcal{A}_x$ is to translate the Fermi surface $E^2 = k_x^2 + k_y^2$ by δt along the horizontal axis. Conservation of energy and momentum immediately leads to a sector of allowed incident angles, as drawn. Analogous reasoning applies for a pure electrostatic barrier (where the Fermi surface in the barrier changes size) or a combination of both. In all cases this geometrical construction immediately yields the transmission sector. It is clear that, whereas in a purely electrostatic barrier the transmission sector is symmetric with respect to normal incidence ($\phi = \pi/2$), in a VP barrier this sector always contains either $\phi = 0$ or π, depending on the relative sign of E and δt. Combining these two cases one can generate
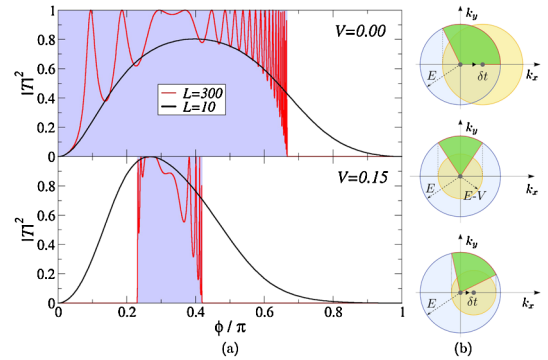

FIG. 2 (color online). Transmission obtained from (5) for $L = 10, 300$, $\delta t = 0.1$, $E = 0.2$ with (bottom) and without (top) gate potential V. On the right we depict the phase space for the cases where only the strain-induced VP is present ($\mathcal{A}_x \neq 0$, $V = 0$), for a pure gate potential ($\mathcal{A}_x = 0$, $V \neq 0$) and for a combination of both ($\mathcal{A}_x \neq 0$, $V \neq 0$). The shaded (green) sectors represent the range of incident angles ϕ which are not filtered by the barrier.

virtually any transmission sector with a single barrier, as exemplified in Fig. 2.

This has immediate applicability in electron beam collimation and lensing, and the effect is easily amplifiable through a series of barriers [13]. In addition, the beam refracted by the barrier can approach or recede from the normal interchangeably by changing the sign of δt. Alternatively, since the transmission sector depends explicitly on E, a suitable geometrical configuration of barriers can be used to filter the energy of the incoming beam. In addition, the suppression of tunneling for certain angular sectors leads to the appearance of a transport gap, as shown in Ref. [15]. Therefore, even though small strain does not lead to a bulk spectral gap, the system exhibits an effective transport gap when the density is below the threshold defined by the overlap of the two Fermi surfaces of Fig. 2(b): if they do not overlap there is no phase space for transmission through the stained region. Within the allowed sector, transmission through wider barriers is additionally characterized by a series of marked resonances where $|T|^2 = 1$, and electron flow is totally unhindered. Such behavior, associated with successive internal reflections, strongly suggests the possibility of confinement.

Confinement.—Dirac electrons are notoriously resilient to conventional confinement strategies on account of the Klein paradox [3]. The fact that our VP barriers exponentially suppress electronic transmission will be further explored to confine Dirac electrons. A confined state inside the barrier has the form

$$\Psi^{\mathrm{I}} = A e^{ik_x x} e^{\kappa y} \begin{pmatrix} 1 \\ e^{\vartheta} \end{pmatrix}, \qquad \Psi^{\mathrm{III}} = D e^{ik_x x} e^{-\kappa y} \begin{pmatrix} 1 \\ e^{-\vartheta} \end{pmatrix},$$

$$\Psi^{\mathrm{II}} = B e^{ik_x x} e^{ik_y y} \begin{pmatrix} 1 \\ e^{i\varphi} \end{pmatrix} + C e^{ik_x x} e^{-ik_y y} \begin{pmatrix} 1 \\ e^{-i\varphi} \end{pmatrix}. \qquad (6)$$

From the wave equation it follows that $E^2 = k_x^2 - \kappa^2 = (k_x - \delta t)^2 + k_y^2$, $k_x = E \cosh\vartheta$, $\kappa = E \sinh\vartheta$, $k_x - \delta t = E \cos\varphi$, $k_y = E \sin\varphi$. From the fact that $E^2 > 0$, this type of solution requires $|k_x - \delta t| < |E| < |k_x|$. This is graphically represented by region 2 in Fig. 3(c). In addition, continuity of the wave function requires that

$$\cot(k_y L) \sin\varphi \sinh\vartheta = 1 - \cos\varphi \cosh\vartheta \qquad (7)$$

be satisfied. When solved for E, Eq. (7) yields a discrete spectrum of energies for each value of k_x: $E_n(k_x)$. Region 2 shown in Fig. 3(c) is therefore characterized by the emergence of *1D channels confined to the barrier region* (quantum wire), and dispersing along k_x. A particular realization of this effect is shown in Fig. 3(a). It is clear from this figure and Eqs. (6) and (7) that such states share all the features of the 1D modes typical of graphene nanoribbons. In particular, at the displaced Dirac point the spectrum scales as $E_n(k_x = \delta t) \approx (n + 1/2)\pi/L$ and, for all purposes related to the electronic states and spectrum, in region 2 this system behaves as a nanoribbon. This applies to the energy scales associated with the confinement gaps
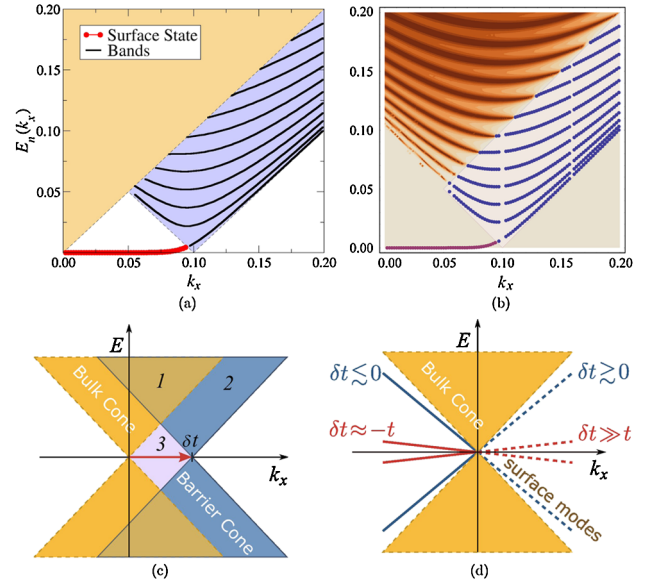

FIG. 3 (color online).   (a) Dispersion of the confined solutions $E_n(k_x)$ for $\delta t = 0.1$ and $L = 200$. (b) A density plot of the transmission $t(E, k_x)$ from Eq. (5) is shown in the upper region (region 1), which is plotted together with the same data as in panel (a). (c) Regions 1, 2, and 3 discussed in the text. (d) Linearly dispersing modes for the narrow barrier discussed in the text.

as well. For example, the gap is roughly $E_g \approx 1/L$ eV nm, so that $L \approx 20$ nm yields a gap of ≈ 50 meV. This is valid as long as $\delta t \gg E_g$, which should be the case for $\delta t/t \sim 10\%$. Hopping variations of this magnitude can be achieved with a local strain of $\sim 5\%$ [18].

Surface modes.—The similarity of a VP barrier with the physics of a nanoribbon achieves its fullest if one notices that surface states are also possible. Just like the edge modes of zigzag nanoribbons, we consider a state localized at the barrier edges. Such state should decay to both sides of $y = 0$ and $y = L$ simultaneously. Consequently we can construct its wave function from Eq. (6) through analytical continuation of k_y to the imaginary axis: $k_x \rightarrow i\kappa'$. The energy will be $E^2 = k_x^2 - \kappa^2 = (k_x - \delta t)^2 - \kappa'^2$, which restricts the space of solutions to the areas outside both Dirac cones [Fig. 3(c)]. The solution for the wave function so constructed leads to a quantization condition analogous to (7) but, since the circular functions are converted to hyperbolic, will admit only one solution, valid precisely when $0 < k_x \le \delta t$ [region 3 of Fig. 3(c)]. In region 3 we then have a single state, whose dispersion is shown in Fig. 3(a). This mode smoothly merges with the lowest state in region 2 and, in the limit of $L \rightarrow \infty$ its energy is given by $E \approx 2(\delta t - k_x)\sqrt{\frac{k_x}{\delta t}} e^{-L(\delta t - k_x)}$, making clear that this mode's energy decays exponentially from the shifted Dirac point towards $k_x = 0$. Inspection of the solution in this limit reveals that the amplitude in one sublattice becomes much smaller than in the other, and one straightforwardly demonstrates that such surface states persist in the limit $L = \infty$ where the problem reduces to a VP step.

The results shown in Fig. 3(a) are symmetric with respect to $E = 0$ [16]. This figure shows that the region 2 ∪ 3, lying outside the continuum of the bulk of the system, supports spatially confined 1D modes, which have the same characteristics as modes in a ribbon, including the presence of surface states. We can now coherently interpret what happens in region 1, in connection with the tunneling calculations described earlier: just as in a conventional potential barrier, the scattering states in region 1 (the bulk continuum) should "feel" the presence of the confined solutions inside the barrier. This manifests itself through the transmission resonances already shown in Fig. 2(a). In fact, when the transmission (7) is plotted in the (E, k_x) plane, we obtain the result shown in region 1 of Fig. 3(b). The darker regions of this density plot correspond to the transmission resonances, which lie in the extrapolation of the confined modes into the bulk continuum.

Narrow limit.—The approach used so far begs revision for the case of very narrow and/or large perturbations in the hopping. The clearest example is the case where L approaches the lattice spacing, so that hopping is perturbed only in one unit cell along $\boldsymbol{u}_y$. Clearly, if $\delta t = -t$ the upper and lower half planes become disconnected and no tunneling is expected. This, however, is not captured by Eq. (5) which assumes overall continuity of the wave function and small perturbations. Since the narrow limit is of interest (e.g., in the case of a tight graphene crease, or a narrow junction between two edges), we tackle it by analyzing the localized perturbation

$$\delta t(\boldsymbol{R}_i, \boldsymbol{n}) = \delta t \delta_{\boldsymbol{n},0} \delta_{Y_i,0} \Rightarrow \mathcal{A}(\boldsymbol{r}) = \hbar v_F \frac{\delta t}{t} \delta(y)\boldsymbol{u}_x. \quad (8)$$

The presence of $\delta(y)$ in (8) imposes a boundary condition at the origin, which, since the wave equation is of 1st order, requires discontinuity of the wave function:

$$\psi^B(0^-) = \eta \psi^B(0^+), \qquad \psi^A(0^+) = \eta \psi^A(0^-), \quad (9)$$

with $\eta = 1 + \delta t/t$. The wave function is naturally discontinuous and, moreover, for $\delta t = -t$ ($\eta = 0$) vanishes in different sublattices at the upper and lower half-plane. Notice that in the case $\delta t = -t$ the system is composed of two independent semiplanes with a zigzag termination. Our BC reproduces the correct BC for these two zigzag semiplanes [10]. The transmission and reflection amplitudes as a function of $\phi = \arg(k_x + ik_i)$ read

$$R = \frac{1 - \eta^2}{\eta^2 - e^{-2i\phi}}, \qquad T = \eta \frac{1 - e^{-2i\phi}}{\eta^2 - e^{-2i\phi}}, \quad (10)$$

with $|R|^2 + |T|^2 = 1$, and $T = 0$ for $\eta = 0$ as expected. The interesting fact about such narrow barriers is that they still support surface modes. Applying the same procedure outlined above to the case (8), one straightforwardly obtains a state that decays exponentially to both sides of the axis $y = 0$. Its dispersion is given by $E(k_x) = \pm v_s |k_x|$ where $v_s = 2|\eta|/(1 + \eta^2)$ and such states exist for $k_x > $

$0(k_x < 0)$ when $\eta^2 > 1(\eta^2 < 1)$. This is a very interesting situation: the perturbation of a single row of hoppings leads to the emergence of linearly dispersing 1D modes that live along the perturbed line. These modes detach from the continuum for small δt, and reach zero energy at $\delta t = -t$, as expected for the two zigzag semiplanes that result in that limit. This is illustrated in Fig. 3(d).

In summary, our approach demonstrates how strain-induced gauge fields can be tailored to generate confined states, quantum wires, and collimation in graphene. Our assumption of a sharp step in (3) is for convenience only: the crucial detail involved in the tunneling suppression is the total variation in the effective gauge field over the edge smearing region. A smearing of the boundaries can be seen as a region with a roughly constant effective magnetic field, which has been shown to exhibit precisely the same phase-space related tunneling suppression [17]. These results, together with the fact that strain has been reliably controlled in graphene [9], open an exciting prospect towards all-graphene electronics.

[1]   A. K. Geim and K. S. Novoselov, Nature Mater. **6**, 183 (2007).
[2]   K. S. Novoselov *et al.*, Science **306**, 666 (2004).
[3]   M. I. Katsnelson, K. S. Novoselov, and A. K. Geim, Nature Phys. **2**, 620 (2006).
[4]   M. Y. Han *et al.*, Phys. Rev. Lett. **98**, 206805 (2007).
[5]   L. A. Ponomarenko *et al.*, Science **320**, 356 (2008).
[6]   E. R. Mucciolo, A. H. Castro Neto, and C. H. Lewenkopf, Phys. Rev. B **79**, 075407 (2009).
[7]   F. Sols, F. Guinea, and A. H. Castro Neto, Phys. Rev. Lett. **99**, 166803 (2007).
[8]   D. Tománek, Physica (Amsterdam) **323B**, 86 (2002).
[9]   Z. H. Ni *et al.*, arXiv:0810.3476.
[10]   A. H. Castro Neto *et al.*, Rev. Mod. Phys. **81**, 109 (2009).
[11]   H. Xu, T. Heinzel, M. Evaldsson, and I. V. Zozoulenko, Phys. Rev. B **77**, 245401 (2008).
[12]   M. R. Masir *et al.*, Phys. Rev. B **77**, 235443 (2008).
[13]   S. Ghosh and M. Sharma, arXiv:0806.2951.
[14]   L. Dell'Anna and A. De Martino, Phys. Rev. B **79**, 045420 (2009).
[15]   M. M. Fogler, F. Guinea, and M. I. Katsnelson, Phys. Rev. Lett. **101**, 226804 (2008).
[16]   Our results are symmetric when $E \rightarrow -E$. When $\delta t \rightarrow -\delta t$ the cone moves in the opposite direction, and our results should be reflected along the axis $k_x = 0$.
[17]   A. De Martino, L. Dell'Anna, and R. Egger, Phys. Rev. Lett. **98**, 066802 (2007).
[18]   V. M. Pereira, A. H. Castro Neto, and N. M. R. Peres, Phys. Rev. B **80**, 045401 (2009).